Implicit atomistic viscosities in smoothed particle hydrodynamics

Marco Ellero,[1,2] Pep Español,[2] and Nikolaus A. Adams[1]
[1]*Lehrstuhl für Aerodynamik, Technische Universität München, 85747 Garching, Germany*
[2]*Departamento de Física Fundamental, UNED, Apartado 60141, 28080 Madrid, Spain*
(Received 18 May 2010; revised manuscript received 6 August 2010; published 5 October 2010)

We consider a standard microscopic analysis of the transport coefficients, commonly used in nonequilibrium molecular dynamics techniques, and apply it to the smoothed particle hydrodynamics method in steady-shear flow conditions. As previously suggested by Posch *et al.* [Phys. Rev. E **52**, 1711 (1995)], we observe the presence of nonzero microscopic (kinetic and potential) contributions to the total stress tensor in addition to its dissipative part coming from the discretization of the Navier-Stokes continuum equations. Accordingly, the dissipative part of the shear stress produces an output viscosity equal to the input model parameter. On the other hand, the nonzero atomistic viscosities can contribute significantly to the overall output viscosity of the method. In particular, it is shown that the kinetic part, which acts similarly to an average Reynolds-like stress, becomes dominant at very low viscous flows where large velocity fluctuations occur. Remarkably, in this kinetic regime the probability distribution function of the particle accelerations is in surprisingly good agreement with non-Gaussian statistics observed experimentally.

DOI: 10.1103/PhysRevE.82.046702 PACS number(s): 47.11.−j

I. INTRODUCTION

Smoothed particle hydrodynamics (SPH) is a meshless particle method able to discretize an arbitrary set of partial differential equations in a Lagrangian framework [1,2]. In spite of its robustness and flexibility, SPH still suffers of problems related to its numerical accuracy. The existence of spurious transport coefficients in the method is well-known and it is usually associated to the occurrence of disordered particle configurations and artificial mixing. This is particularly evident for high Reynolds number flows where the particle inertia is large, effectively limiting the applicability of standard SPH for accurate direct numerical simulations (DNS) of turbulent flows [3].

In [4], a systematic study of the spurious SPH viscosities was performed and a direct connection with the numerical SPH particle diffusion was highlighted. Alternatively, in [5,6] a different approach was pursued in order to characterize the transport coefficients: by invoking the isomorphism linking the SPH equations describing an inviscid fluid with the ones governing the motion of an atomistic Lucy fluid, the authors performed nonequilibrium molecular dynamics (NEMD) simulations of the latter under homogenous shear flow to deduce the spurious transport coefficients of SPH. The presence of two *atomistic* viscosities in a thermostated Lucy fluid, analogous to the microscopic kinetic and potential ones, was reported. Intrinsic viscosity as well as other transport coefficients (i.e., thermal conductivity) [7] were later observed and their dependence on applied shear rate and averaged velocity fluctuations (kinetic temperature) numerically quantified.

An interesting point highlighted by Hoover was that the continuum interpretation of the two microscopic viscosities is very different. Indeed, although the potential one has no continuum analog, the kinetic viscosity which is based on particle velocity fluctuations, acts formally as a negative averaged Reynolds stress in standard turbulence closures [8]. It is therefore very important to separate the two contributions in order to quantify the different source of errors and to understand whether intrinsic SPH dissipative mechanisms can be used as sub particle-scale (SPS) turbulent models in the spirit of implicit large eddy simulations (ILES) [9].

In this paper, we study the behavior of the SPH spurious viscosity under homogeneous shear flow differentiating the several contributions. Unlike the study made in [5], here no microscopic Nosé-Hoover (or similar) thermostat is employed to achieve a nonequilibrium stationary state. The presence of an input viscosity through the SPH discretization of the full Navier-Stokes equations [10,11] allows to stabilize the simulations without imposing *a priori* a specified level of velocity fluctuations. As a consequence, particle velocity fluctuations are unconstrained, emerge naturally and eventually become dominant in very large Reynolds number flows: the corresponding regime is denoted in this paper as *kinetic regime*. The behavior is studied under different choice of the Mach number and it is found to be predominant in strongly compressible situations. In this latter case, we observe a kind of phase transition in the averaged fluid density corresponding to the onset of the kinetic regime. Although the statistics of the particle velocity fluctuations remain Gaussian, the probability distribution function of the corresponding accelerations has a stretched exponential shape increasing its kurtosis as the effective Reynolds number increases. This intermittency feature has been already observed in Voronoi simulations [16] and, despite a difference in the Mach number, it is in surprisingly good qualitative agreement with recent experimental measurements of Lagrangian particle accelerations in fully developed turbulence [17,18] and direct numerical simulations [19].

II. SPH METHOD

SPH is a particle method which makes use of a kernel function to interpolate any function f at the position $\mathbf{r}$, by using its values defined at a discrete set of disordered points, that is

$$\langle f(\mathbf{r})\rangle \simeq \sum_j \frac{1}{d_j} f_j w(|\mathbf{r}-\mathbf{r}_j|,h), \tag{1}$$

where $f_j \equiv f(\mathbf{r}_j)$, $w(r,h)$ is the kernel and d_j is the particle number density at the position $\mathbf{r}_j$ defined as $d_j = \Sigma_k w_{kj}$ being $w_{kj} = w(|\mathbf{r}_k - \mathbf{r}_j|,h)$. $w(r,h) = w(|\mathbf{r}|,h)$ is an even, normalized, bell-shaped interpolation function with compact support equal to h. Many choice are possible for w: in this work we consider the so-called *Lucy kernel* [1].

$$w(\mathbf{r},h) = w_0 \begin{cases} (1+3r/h)(1-r/h)^3, & r/h < 1 \\ 0, & r/h \geq 1 \end{cases}, \tag{2}$$

where $w_0 = 5/(\pi h^2)$ in 2D. It can be shown that by convolving the Navier-Stokes equations with the kernel w, a corresponding set of ordinary differential equations for a system of particles can be obtained. For example, one possible SPH discretization of the Navier-Stokes equations is

$$\dot{\mathbf{p}}_i = \sum_j (\mathbf{F}_{ij}^{cons} + \mathbf{F}_{ij}^{diss}), \tag{3}$$

where $\mathbf{F}_{ij}^{cons}$ is a conservative interparticle force which reads [10]

$$\mathbf{F}_{ij}^{cons} = -m^2 \left(\frac{p_i}{\rho_i^2} + \frac{p_j}{\rho_j^2} \right) w'_{ij} \mathbf{e}_{ij}, \tag{4}$$

m is a constant particle mass, $\rho_i = m d_i$ is mass density associated to particle i, p_i its pressure, $\mathbf{e}_{ij} = \mathbf{r}_{ij}/r_{ij}$ the unit vector joining particles i and j and $w'_{ij} = \partial_r w(r,h)|_{r=r_{ij}}$. With this definition of the particle forces, a second-order Lagrangian discretization of the Euler equations is recovered. Furthermore, in the case of a viscous fluid, an additional dissipative interparticle contribution is considered which in 2D reads

$$\mathbf{F}_{ij}^{diss} = \frac{1}{3} \eta_0 m^2 \frac{w'_{ij}}{\rho_i \rho_j r_{ij}} [4(\mathbf{e}_{ij} \cdot \mathbf{v}_{ij})\mathbf{e}_{ij} + 5\mathbf{v}_{ij}], \tag{5}$$

where $\mathbf{v}_{ij} = \mathbf{v}_i - \mathbf{v}_i$ is the relative particle velocity. Analogously, a second-order discretization of the viscous terms in the Navier-Stokes equations characterized by a shear viscosity η_0 is obtained [11].

In order to close the system of equations, the following equation of state:

$$p(\rho) = p_0 \left[\left(\frac{\rho}{\rho_0} \right)^\gamma - 1 \right] \tag{6}$$

is usually considered, where ρ_0 is the equilibrium mass density and γ is a model parameter; the resulting liquid speed of sound is $c_s = (\gamma p_0/\rho_0)^{1/2}$.

III. MICROSCOPIC ANALYSIS

The atomistic transport coefficients can be evaluated in molecular dynamics simulation under equilibrium conditions at constant temperature by estimating time correlation functions and using the linear response theory, i.e., obtaining the Green Kubo relations [12]. The other way considered in NEMD, is to apply a large perturbation creating a flow of momentum in the material under study and measuring the resulting pressure tensor. In the specific case of the viscosity, a simple periodic shear flow is created by applying the so-called Lees-Edwards boundary conditions [13]. This is a modification of the standard periodic boundary conditions obtained by moving periodic upper and lower simulation boxes with constant velocities $V = \pm (1/2)\dot{\gamma} L$, where L is the box size and $\dot{\gamma}$ is the desired shear rate.

In the case of SPH, the instantaneous microscopic pressure tensor $\mathbf{P}$ is evaluated as the local average of momentum flux by using

$$\mathbf{P} = \frac{1}{V} \left(m \sum_i \mathbf{c}_i \mathbf{c}_i + \sum_{i,j>i} \mathbf{r}_{ij} \mathbf{F}_{ij}^{cons} + \sum_{i,j>i} \mathbf{r}_{ij} \mathbf{F}_{ij}^{diss} \right) \tag{7}$$

where $\mathbf{c}_i$ is the particle velocity in the comoving frame, i.e., $\mathbf{c}_i = (c_i^x, c_i^y) = (v_i^x, v_i^y) - (\dot{\gamma} y_i, 0)$ and y_i is the particle coordinate in the direction normal to the shear (see derivation in the Appendix). The total liquid shear viscosity η is evaluated by time-averaging the off diagonal components of the pressure tensor and dividing them by the applied shear rate $\dot{\gamma}$ as follows:

$$\eta = -\frac{\langle P_{xy} \rangle}{\dot{\gamma}} = \eta_{\text{kin}} + \eta_{\text{pot}} + \eta_{\text{diss}}, \tag{8}$$

where $\langle .. \rangle$ denotes here the time average. In the previous expression, the kinetic viscosity is $\eta_{\text{kin}} = \frac{1}{V\dot{\gamma}} \langle -m \Sigma_i c_i^x c_i^y \rangle$. Analogously, the potential and dissipative contributions are calculated starting from the corresponding off diagonal terms in Eq. (7).

Notice that for consistency, η_{diss} extracted from the simulations should be exactly equal to η_0 (input). Whereas this viscosity corresponds to the specific dissipation adopted in the continuum model, the remaining ones (kinetic and potential) are specific of the particulate nature of the method and we regard them as *atomistic*.

IV. SIMULATIONS RESULTS

We consider a viscous SPH fluid defined on a unbounded domain and apply the Lees-Edwards periodic boundary conditions to generate a nonequilibrium steady-state shearing flow. We consider a square simulation box ($L=1$) and apply a uniform shearing motion by translating upper and lower periodic box images, respectively, with velocities $V_0 = \pm \dot{\gamma} L/2$ where $\dot{\gamma}=1$. Two different speeds of sound $c_s = 10, 0.33$ are investigated, which define Mach numbers based on the velocity difference ($\Delta V = 2V_0$), $\text{Ma} = \Delta V/c_s = 0.1, 3.0$. Nevertheless, local Mach numbers based on the particle fluctuating velocities can be occasionally larger in the kinetic regime. The equilibrium mass density ρ_0 is set to 1 and a set of simulations corresponding to values of the input viscosities η_0 in $[10^{-5}:1]$ are performed. In order to remove artificial effects due to the initial lattice configuration, preruns were considered in each case to relax it. When an equilibrated disordered state was achieved, the shear perturbation was applied and the results extracted. In order to exclude effects due to the finite time step used in the integrator, simulations were performed first with $\Delta t = 2.3 \times 10^{-4}, 2.3 \times 10^{-3}$ (respectively, for Ma=0.1, 3.0) and then

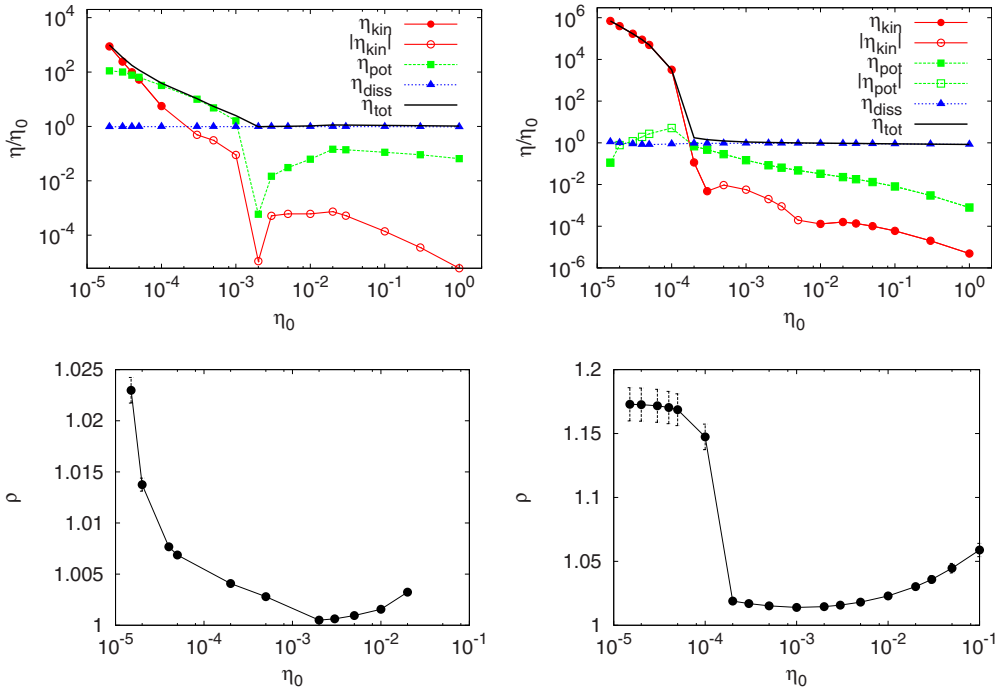

FIG. 1. (Color online) Top: contribution of atomistic viscosities to the total SPH viscosity in a simple shear flow: (Left) Ma=0.1; (Right) Ma=3.0. Bottom: averaged fluid density vs. η_0: (Left) Ma=0.1; (Right) Ma=3.0

repeated with reduced time steps showing identical results. In order to produce reliable statistics, simulations where continued for more than 10^6 time steps once the steady state was achieved.

We study the influence of the input viscosity η_0 on the output viscosities and check explicitly under which mechanism the averaged output viscosity deviates from its given input value. An exact numerical method should give $\eta = \eta_{\text{diss}} = \eta_0$ for every η_0. Figure 1 shows the different contributions to the total SPH viscosity normalized by the input model viscosity η_0 and corresponding averaged density for Ma=0.1 (left) and Ma=3.0 (right). Number of particles was $N=32^2$ and particle overlap of the Lucy kernel was $\kappa=3$ corresponding to an averaged number of 28 neighbors per particle.

First we noticed that in both cases the dissipative viscosity η_{diss} is in good agreement with the input value η_0 overall the range considered. This observation is important because it rules out the dissipative part of the SPH dynamics as main source of error in the determination of the fluid viscosity. Main errors must therefore be predominantly associated with the two additional microscopic contributions η_{pot} and η_{kin}.

In the regime of large input viscosities $\eta_0 \in [10^{-2}:1]$, the kinetic contribution η_{kin} is very small in magnitude (less than 0.1% of η_0) and is found to be very weakly dependent on both number of particles N and average number of neighbors. Nevertheless, the potential contribution η_{pot} is not negligible specially at Ma=0.1 ($\approx$10% of η_0). Furthermore, whereas η_{diss} is found to be resolution independent (similar to η_{kin}), η_{pot} is strongly affected by the number of neighboring particles used in the SPH interpolations and we have explicitly verified that it tends to zero by increasing the cutoff radius h of the Lucy kernel as already observed in [4]. This observation enforces the interpretation of η_{pot} as spurious numerical viscosity related to quadrature errors in the discrete estimates of the continuum integrals made in SPH [14]. η_{pot} is therefore directly related to the 'particulate nature' of the method, which on the continuum level must be considered artificial.

For decreasing values of the input viscosity, the relative potential contribution increases crossing the constant line equal to 1 for $\eta_0 \approx 10^{-3}$ for Ma=0.1 and at $\eta_0 \approx 2\times 10^{-4}$ for Ma=3.0. In order to perform accurate SPH simulations it is therefore necessary to reduce η_{pot} below a certain acceptable threshold which is controlled by the particle overlap. Notice also that the *potential* error is present only when a disordered particle configuration occurs. In the special case of particles

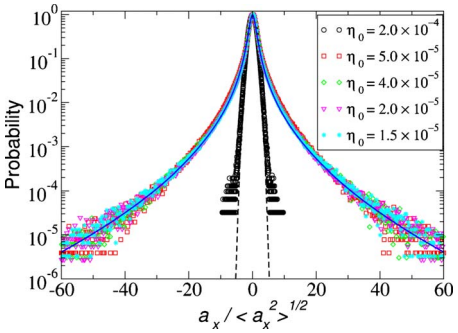

FIG. 2. (Color online) Acceleration distribution: probability distribution function of the x-component of the particle accelerations corresponding to different fluid viscosities at Ma=3. Black dotted line represents a Gaussian fit with $\sigma=1.0$. Blue line represents a parameterization of the smallest viscosity using the function $P(a) = \exp(-a^2/((1+(a\beta/\sigma)^\gamma)\sigma^2))$ [17], with $\sigma=1$, $\beta=0.63$ and $\gamma=1.56$.

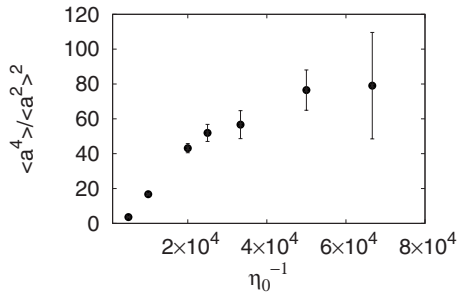

FIG. 3. Kurtosis of the distribution plotted vs. η_0^{-1}. Its value for Gaussian statistics is 3.

placed on a square grid, the sums involving $\mathbf{F}_{ij}^{cons}$ in Eq. (7) vanish identically. This observation agrees with the well-known fact that SPH produces more accurate results when particles lie on a lattice and the idea has been exploited in a number of recent remeshing SPH techniques [3,15].

A second important observation from Fig. 1 is that, in the small viscosity regime, the dominant viscous contribution is purely kinetic. The behavior is more pronounced at large Mach number where for $\eta_0 \approx 10^{-4}$, η_{kin} is already more than 1000 times larger than η_0. We should remember that the value of η_{kin} is strictly related to the level of fluctuations present in the velocity field and, unlike thermostat-based NEMD methods, here it is not constrained. The behavior of η_{kin} is therefore quite peculiar, being naturally small at very low effective Reynolds number flows and becoming dominant in the opposite limit, a typical feature of turbulent energy transfer. Stimulated by this analogy, we decided to look in more details at the SPH fluctuating field statistics by means of which the kinetic dissipation takes place.

Kinetic regime and non-Gaussian statistics

After evaluating the particle velocity probability distribution function (pdf) in both, weakly compressible and highly compressible cases, we did not observe relevant deviations from Gaussian behavior. Nevertheless, stretched exponential tails are observed in the pdf of Lagrangian accelerations, see Fig. 2, in agreement with recent experimental measurements [17,18], highly resolved DNS [19] and also confirmed by analytical theories as the multifractal or simple vortex models [20,21]. In Voronoi-based simulations [16] a similar intermittent behavior was also reported.

More specifically, in our simulation non-Gaussian acceleration tails were exclusively observed in the kinetic regime at Ma=3 where η_{kin} widely overwhelms the input viscosity. This kinetic regime develops approximately for $\eta_0 \leq 1 \times 10^{-4}$ and corresponds to a sort of phase-transition in the average fluid density $\langle \rho \rangle$ as it can be seen in the Fig. 1 (bottom-right). On the other hand, neither transition in the density nor stretched tails in the acceleration pdf were observed for the case Ma=0.1. It is also quite remarkable that the pdf's kurtosis $\langle a^4 \rangle / \langle a^2 \rangle$ vs. η_0^{-1} depicted in Fig. 3 is in surprisingly good agreement with that obtained from experimental measurements of passive tracers in [17].

In [18], the intermittency of Lagrangian accelerations was associated to the presence of coherent small-scale vortical structures in which tracer particles are occasionally trapped, undergoing large centripetal accelerations. Evidence of strong correlations between vortical structures and high acceleration events was reported also in [19].

In Fig. 4 we have plotted snapshots of some hydrodynamic fields at a given time for the case corresponding to Ma=3 for $\eta_0=10^{-4}$ just above the transition in the density (top figures) and for $\eta_0=2\times10^{-4}$ shortly below the transition. Before the transition, the density field (bottom-right) is only slightly fluctuating and the corresponding values of the particle acceleration are quite small (bottom-center). Also, the velocity field (bottom-left) although exhibiting small fluctuations, it is close with the linear velocity profile applied through the Lees-Edwards boundary conditions.

The top figures correspond to the case where the typical stretched tails in the acceleration pdf were observed. The top-left plot depicts a snapshot of the contours of the velocity field which now appears to be fully chaotic. The high-acceleration events are associated to typical localized bursts showed in the top-center plot of Fig. 4 which now reach maximal magnitudes up to 40 times larger than in the previous case. In order to understand the origin of these large particle accelerations, similar to what done in [19], we have tried to correlate $a(x,y)$ with the vorticity field $\omega(x,y)$ evaluated from our simulations but without success. Rather, strong correlation was found between a and the density field ρ, Fig. 4 (top-right), suggesting that large pressure gradients causing expanding/contracting flows, rather than coherent vortical structures, are the main responsible of the observed non-Gaussian behavior. Furthermore, bursts are not transported but appear to be created/destroyed locally in a shocklike fashion. It should be noticed that the phenomenology observed in [17,18] corresponds to an incompressible fluid flow. In highly compressible fluids, velocity fluctuations become comparable to the speed of sound producing shocklets, localized fluid expansions/contractions and the entire turbulent phenomenology can be quite different. In [22] evidence of shocklets created by a supersonic fluctuating velocity field was reported. Interestingly similar structures have been observed in our simulations and are responsible for an enhanced dissipation implicitly contained in the method. Further numerical investigation is currently under work in order to assess the applicability of the kinetic SPH viscosity as a sub-particle-scale model in compressible turbulence. Specifically, it would be very helpful to understand the phenomenon of non-Gaussian Lagrangian acceleration statistics in highly compressible turbulent flows. Non-Gaussian statistics in fully developed turbulent flows have been recently analyzed in the framework of the Tsallis statistical ensemble [23] and a multifractal model (MF) for the acceleration pdf developed which produces quantitative agreement with DNS and experiments [20]. Comparisons of the SPH acceleration statistics with the MF model in a forced three-dimensional turbulent case are currently under way and the results will be presented elsewhere.

V. CONCLUSIONS

A microscopic analysis of the transport coefficients similar to what is done in NEMD simulations has been applied to

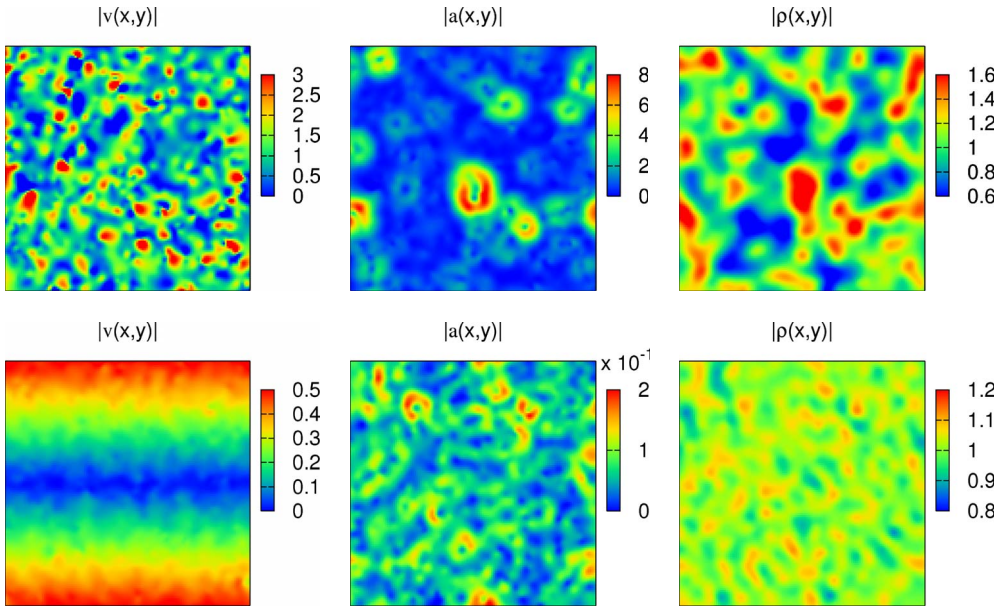

FIG. 4. (Color online) Snapshot of the hydrodynamic fields corresponding to Ma=3. Velocity (left), acceleration (center) and density field (right). Top plots correspond to $\eta_0=10^{-4}$ (just above the density transition); Bottom plots correspond to $\eta_0=2\times10^{-4}$ (just below the density transition)

the macroscopic SPH method in order to extract its implicit atomistic viscosities. The spurious potential viscosity, which is related to stochastic particle locations, represents a non-negligible part of the total measured output viscosity in the high viscous regime. There is no analogous physical mechanism in the continuum and therefore it is regarded as spurious particle-size dependent discretization error. Oppositely, the kinetic contribution, related to stochastic particle velocities, corresponds to an average Reynolds-like stress and dominates at very small input viscosity. When the kinetic regime is achieved, the pdf of the particle accelerations exhibits non-Gaussian behavior similar to that observed in the measurements of particle tracers dynamics in fully developed turbulent flows. Areas of large accelerations cannot be, however, associated to the presence of coherent vortical structures as experimentally observed in incompressible fluids. Nevertheless, statistics of turbulent flows are surprisingly well captured by the method when applied to highly compressible flows. In order to determine whether these implicit kinetic viscosity can reproduce some phenomenology of turbulence, our investigations are currently focusing in two directions: from one side the statistical behavior of the system needs to be more carefully studied, namely higher order Lagrangian structure functions need to be determined; on the other hand, following the philosophy of Implicit Large Eddy Simulations, energy spectra of homogenous turbulence obtained from under-resolved simulations are currently under investigation and should help to clarify the possible use of the kinetic SPH viscosity as a SPS model.

ACKNOWLEDGMENTS

Financial support from the Deutsche Forschungsgemeinschaft (DFG) via the grant No. EL503/1-1 is gratefully acknowledged.

APPENDIX: MICROSCOPIC PRESSURE TENSOR

Consider a system of N particles moving according to the equations of motion

$$\dot{\mathbf{r}}_i = \mathbf{v}_i$$

$$m_i\dot{\mathbf{v}}_i = \sum_j \mathbf{F}_{ij} \tag{A1}$$

where $\mathbf{F}_{ij}$ is the pairwise force (that may in principle depend on the velocities).

The mass and momentum density fields of a system of particles are defined by

$$\hat{\rho}(\mathbf{r},t) = \sum_i m_i\delta[\mathbf{r}-\mathbf{r}_i(t)]$$

$$\hat{\mathbf{g}}(\mathbf{r},t) = \sum_i m_i\mathbf{v}_i\delta[\mathbf{r}-\mathbf{r}_i(t)] \tag{A2}$$

We may introduce the velocity field as

$$\hat{\mathbf{g}}(\mathbf{r},t) = \hat{\rho}(\mathbf{r},t)\hat{\mathbf{v}}(\mathbf{r},t) \tag{A3}$$

(use a peaked Gaussian instead of a Dirac delta function in order to avoid the singularities).

If we take the time derivatives of these fields, we get the Irving-Kirkwood results [24]

$$\partial_t\hat{\rho}(\mathbf{r},t) = -\nabla\cdot\sum_i m_i\mathbf{v}_i\delta(\mathbf{r}-\mathbf{r}_i(t)),$$

$$\partial_t \hat{\mathbf{g}}(\mathbf{r},t) = -\nabla\cdot\sum_i m_i\mathbf{v}_i\mathbf{v}_i\delta[\mathbf{r}-\mathbf{r}_i(t)] + \sum_{ij}\mathbf{F}_{ij}\delta(\mathbf{r}-\mathbf{r}_i)$$
$$= -\nabla\cdot\left\{\sum_i m_i\mathbf{v}_i\mathbf{v}_i\delta[\mathbf{r}-\mathbf{r}_i(t)] + \frac{1}{2}\sum_{ij}\mathbf{F}_{ij}\mathbf{r}_{ij} \times\int_0^1 d\epsilon\,\delta(\mathbf{r}-\mathbf{r}_i+\epsilon\mathbf{r}_{ij})\right\}$$
$$= -\nabla\cdot\hat{\rho}\mathbf{v}\mathbf{v} - \nabla\hat{\mathbf{\Pi}}, \tag{A4}$$

where we have introduced the microscopic stress tensor field as

$$\hat{\mathbf{\Pi}}(\mathbf{r}) = \sum_i m_i\mathbf{c}_i\mathbf{c}_i\delta[\mathbf{r}-\mathbf{r}_i(t)] + \frac{1}{2}\sum_{ij}\mathbf{F}_{ij}\mathbf{r}_{ij}\int_0^1 d\epsilon\,\delta(\mathbf{r}-\mathbf{r}_i+\epsilon\mathbf{r}_{ij}), \tag{A5}$$

where $\mathbf{c}_i=\mathbf{v}_i-\mathbf{v}(\mathbf{r}_i)$ is the peculiar velocity, and $\mathbf{v}(\mathbf{r})$ is the average of the velocity field $\hat{\mathbf{v}}$. The microscopic stress tensor field $\hat{\mathbf{\Pi}}(\mathbf{r})$ is a function of the particle positions and velocities.

In situations where we expect that the stress tensor field is homogeneous and independent of space, we may take a space average and consider the following microscopic stress tensor

$$\hat{\mathbf{\Pi}} = \frac{1}{V}\int d\mathbf{r}\mathbf{\Pi}(\mathbf{r}) = \frac{1}{V}\left(\sum_i m_i\mathbf{c}_i\mathbf{c}_i + \frac{1}{2}\sum_{ij}\mathbf{F}_{ij}\mathbf{r}_{ij}\right), \tag{A6}$$

where the space average kills the delta functions. This is the microscopic expression of the stress tensor valid for homogeneous situations.

The *macroscopic* hydrodynamic equations emerge from the above *microscopic* equations by an statistical average and the use of the local equilibrium assumption. In this way, the stress tensor becomes [without a hat to distinguish it from the microscopic stress tensor in Eq. (A5)]

$$\mathbf{\Pi}(\mathbf{r}) = P(\mathbf{r})\mathbf{1} - \eta(\nabla\mathbf{v}+\nabla\mathbf{v}^T) + -\left(\zeta-\frac{2\eta}{3}\right)(\nabla\cdot\mathbf{v})\mathbf{1}, \tag{A7}$$

which now depends on $\rho,\mathbf{v}$, giving a closed form for the hydrodynamic equations. If we introduce the velocity gradient tensor $\dot{\boldsymbol{\gamma}}$ and take $\zeta=0$ for simplicity, we will have

$$\dot{\boldsymbol{\gamma}} \equiv \nabla\mathbf{v}(\mathbf{r}),$$

$$\mathbf{\Pi}(\mathbf{r}) = P(\mathbf{r})\mathbf{1} - \eta(\dot{\boldsymbol{\gamma}}+\dot{\boldsymbol{\gamma}}^T) + \frac{2\eta}{3}\mathrm{Tr}\dot{\boldsymbol{\gamma}}\mathbf{1}. \tag{A8}$$

A shear flow in 2D is defined by the following average fields

$$P(\mathbf{r}) = P_0,$$

$$\mathbf{v}(\mathbf{r}) = \dot{\boldsymbol{\gamma}}\cdot\mathbf{r} = (\gamma y, 0), \tag{A9}$$

where

$$\dot{\boldsymbol{\gamma}} = \begin{pmatrix} 0 & \gamma \\ 0 & 0 \end{pmatrix}. \tag{A10}$$

The average stress tensor that corresponds to this flow will be, from (VII)

$$\mathbf{\Pi} = P_0\mathbf{1} - \eta(\dot{\boldsymbol{\gamma}}+\dot{\boldsymbol{\gamma}}^T), \tag{A11}$$

which is position independent. Equation (A6) and (A7) allow one to compute the viscosity from particle simulations.

[1] L. B. Lucy, Astron. J. **82**, 1013 (1977).
[2] R. A. Gingold and J. J. Monaghan, Mon. Not. R. Astron. Soc. **375**, 181 (1977).
[3] A. K. Chaniotis, D. Poulikakos, and P. Koumoutsakos, J. Comput. Phys. **182**, 67 (2002).
[4] J. C. Lombardi, A. Sillis, F. A. Rasio, and S. L. Shapiro, J. Comput. Phys. **152**, 687 (1999).
[5] H. A. Posch, W. G. Hoover, and O. Kum, Phys. Rev. E **52**, 1711 (1995).
[6] O. Kum, Ph.D. thesis, University of California Davis/Livermore, 1995.
[7] W. G. Hoover and H. A. Posch, Phys. Rev. E **54**, 5142 (1996).
[8] S. B. Pope, *Turbulent Flows* (Cambridge University Press, Cambridge, England, 2000).
[9] S. Hickel, N. A. Adams, and J. A. Domaradzki, J. Comput. Phys. **213**, 413 (2006).
[10] P. Español and M. Revenga, Phys. Rev. E **67**, 026705 (2003).
[11] M. Ellero, M. Serrano, and P. Español, J. Comput. Phys. **226**, 1731 (2007).
[12] W. G. Hoover, *Smoothed Particle Applied Mechanics* (World Scientific Press, Singapore, 2006).
[13] M. P. Allen and D. J. Tildesley, *Computer Simulation of Liquids* (Oxford Scientific Publication, New York, 1987).
[14] N. J. Quinlan, M. Basa, and M. Lastiwka, Int. J. Numer. Methods Eng. **66**, 2064 (2006).
[15] S. Børve, M. Omang, and J. Trulsen, J. Comput. Phys. **208**, 345 (2005).
[16] M. Serrano, P. Español, and I. Zuñiga, J. Stat. Phys. **121**, 133 (2005).
[17] A. L. La Porta, G. A. Voth, A. M. Crawford, J. Alexander, and E. Bodenschatz, Nature (London) **409**, 1017 (2001).
[18] F. Toschi and E. Bodenschatz, Annu. Rev. Fluid Mech. **41**, 375 (2009).
[19] S. Lee and C. Lee, Phys. Rev. E **71**, 056310 (2005).
[20] T. Arimitsu and N. Arimitsu, Physica D **193**, 218 (2004).
[21] M. Wilczek, F. Jenko, and R. Friedrich, Phys. Rev. E **77**, 056301 (2008).
[22] R. Samtaney, D. I. Pullin, and B. Kosovic, Phys. Fluids **13**, 1415 (2001).
[23] T. Arimitsu and N. Arimitsu, J. Phys. A **33**, L235 (2000).
[24] J. H. Irving and J. G. Kirkwood, J. Chem. Phys. **18**, 817 (1950).